

Nanoscale

Accepted Manuscript



This is an *Accepted Manuscript*, which has been through the Royal Society of Chemistry peer review process and has been accepted for publication.

Accepted Manuscripts are published online shortly after acceptance, before technical editing, formatting and proof reading. Using this free service, authors can make their results available to the community, in citable form, before we publish the edited article. We will replace this *Accepted Manuscript* with the edited and formatted *Advance Article* as soon as it is available.

You can find more information about *Accepted Manuscripts* in the [Information for Authors](#).

Please note that technical editing may introduce minor changes to the text and/or graphics, which may alter content. The journal's standard [Terms & Conditions](#) and the [Ethical guidelines](#) still apply. In no event shall the Royal Society of Chemistry be held responsible for any errors or omissions in this *Accepted Manuscript* or any consequences arising from the use of any information it contains.



Green Microwave Switching from Oxygen Rich Yellow Anatase to Oxygen Vacancy Rich Black Anatase TiO₂ Solar Photocatalyst Using Mn (II) as 'Anatase Phase Purifier' †

Received 00th January 20xx,
Accepted 00th January 20xx

DOI: 10.1039/x0xx00000x

www.rsc.org/

Sanjay G. Ullattil, Pradeepan Periyat*

Green and rapid microwave syntheses of 'Yellow oxygen rich' (YAT-150) and 'Black oxygen vacancy rich' (BAT-150) anatase TiO₂ nanoparticles are reported for the first time. YAT-150 was synthesized using titanium (IV) butoxide and water as only precursors. The *in situ* precursor modification by Mn (II) acetate switched the anatase TiO₂ from YAT-150 to BAT-150. The entry of Mn²⁺ into the crystal lattice of anatase TiO₂ paved the way to peak texturing in the existing peak orientations along with origin of three new anatase TiO₂ peaks in (103), (213) and (105) directions. As synthesized ultra-small (~5 nm) yellow and black anatase TiO₂ nanoparticles were found to be two fold and four fold photoactive than the commercially available photocatalyst Degussa-P25 under sunlight illumination.

chemical/heat treatment for the removal of template to obtain pure TiO₂ phase.⁹

Introduction

TiO₂ is one of the most investigated materials around the world owing to its extraordinary chemical stability, low toxicity and wide band gap energy, enables it to serve as an unambiguously accepted remarkable smart material for the contemporary society.¹ Among the three phases, anatase, rutile and brookite of TiO₂, anatase is the most important key player that leads to successful environmental and technological applications such as in photocatalysis,² dye sensitized solar cells,³ electrochromic displays⁴ and self-cleaning fabrics.⁵ However, anatase TiO₂ fails to absorb the entire spectrum of natural sunlight that consists of 5% UV (200-400 nm), 43% visible (400-700 nm) and 52% of infrared (700-2500 nm) regions⁶ due to its higher band gap energy 3.2 eV corresponding to 388 nm. Metal doping was successfully put into effect for increasing absorption maxima and thereby developing efficient photocatalysis.⁷ However, this strategy affected the phase purity of anatase by forming secondary impurities (e.g. Al₂TiO₅, CeTi₄O₂₄ and Ce₂Ti₂O₇) which has limited its photocatalytic efficiency.⁸ Since the drawbacks of metal doping have been proposed, non-metal doping has got a much more attention which has broadened the absorption range from UV to visible region and simultaneous decrease in band gap energy. However, this method required expensive chemicals, templates for structure direction and harsh

Hence synthesizing TiO₂ as a sunlight harvester that can absorb the entire solar spectrum from UV to IR region by a rapid strategy is still unknown. If TiO₂ is in an oxygen vacancy rich environment, a substantial positive absorption shift occurs, that can facilitate absorption even at IR region. Consequently the colour of TiO₂ will be obviously black.^{10,11} Very recently oxygen richness and oxygen vacancy richness in TiO₂ have found the impetus for inducing optical properties and thereby reinforcing effective photocatalysis.¹⁰⁻¹³ However, the use of oxygen rich chemicals such as H₂O₂ and high temperature implementation can't notably alter the oxygen richness in anatase TiO₂ nanocrystals.¹³ For certain, inducing oxygen vacancy richness (Ti³⁺ doping) in such an oxygen rich environment is extremely difficult. In this study we are introducing for the first time a clean, cost effective and eco-friendly microwave synthesis of such a 'yellow oxygen rich' (YAT-150) and 'black oxygen vacancy rich' (BAT-150) anatase TiO₂ nanoparticles which can effectively absorb energy from UV to IR region of the solar spectrum by *in situ* modification of the precursor titanium butoxide using Mn (II) acetate as an 'anatase phase purifier' within a five minute reaction time.

Experimental

Materials. Titanium (IV) butoxide, 97% (Sigma-aldrich), isopropanol, extra pure, AR (Merck), manganese acetate tetrahydrate, extra pure, AR (Sisco Research Laboratories, India), methylene blue (Qualigens, India) were used as

Department of Chemistry, University of Calicut, Kerala, India- 673 635.

Email: pperiyat@uoc.ac.in

Tel: +919746602652

† Electronic Supplementary Information (ESI) available: Photographs of YAT-150 and BAT-150, wide range XPS, SEM images, EDX and UV-Visible absorption spectra of degradation of methylene blue using as synthesized samples and Degussa-P25 are included.

received without further purification. In all reactions deionized water was used.

Synthetic Procedure. For the synthesis of BAT-150 titanium butoxide, 0.2 M (6.8g) was dissolved in 100 mL isopropanol under room temperature. The above solution was stirred at 1200 rpm for 10 minutes and 0.02 M manganous acetate solution (0.2451 g in 50 ml water) was added in small quantity (5 mL) for hydrolysis and doping simultaneously. Stirring was continued for further 30 minutes under same conditions. The reaction mixture obtained was subjected to microwave irradiation for 5 minutes at 150 °C with 1200 rpm using Anton Paar monowave-300 microwave synthesis reactor. The reaction mixture was then cooled to 55 °C. For YAT-150 synthesis, 50 ml water was alone added by replacing 10% manganese acetate solution. Both the samples were dried at 80 °C. The samples were named as YAT-150 (anatase sample which is yellow coloured) and BAT-150 (Mn²⁺ modified anatase sample which is black coloured). A schematic illustration of the synthetic procedure is shown in Figure 1.

Photocatalysis. 0.01599 g of methylene blue (10⁻⁴ M) was made up to 500 mL in a standard flask to get an intense blue coloured dye solution. 50 mL of the prepared methylene blue dye solution was taken in a beaker. Added 0.1g of the TiO₂ nanoparticles to the dye solution prior to the dark adsorption analysis.

Dark Adsorption Analysis. To assess the extent of dye adsorption and to remove the error due to initial adsorption effect, the dye solution was mixed with the photocatalyst and it was stirred for 2 hrs in the UV photoreactor in the absence of light. The UV-Vis absorption spectra of methylene blue before and after were recorded. There is no noticeable change in absorption value of MB in presence of YAT-150 and BAT-150 whereas Degussa-P25 has shown a decrease in absorption value (Figure S1). This step can eliminate any error due to initial adsorption effect. After stirring, it was irradiated under direct sunlight/UV illumination with constant stirring. The degradation was monitored by taking 3 ml aliquots at certain time intervals. To eliminate the error due to scattering the solution taken were centrifuged for 30 minutes prior to the photocatalytic activity measurements.

Characterization. The yellow and black anatase TiO₂ samples were characterized using XRD, FTIR spectroscopy, UV-Visible spectroscopy, XPS, SEM and TEM. X-ray diffraction patterns was recorded using Rigaku diffractometer in the diffraction angle range 2θ = 20-70° using Cu-Kα radiation. The UV-Visible absorbance spectra were obtained from Jasco-V-550-UV/VIS spectrophotometer and FTIR spectra measurements were done using Jasco-FT/IR-4100 spectrophotometer. XPS was recorded with Axis Ultra Kratos Analytical, UK with Al-Kα (1486.6 eV) source. Particle morphologies were examined by SEM and TEM using Hitachi-Su field emission scanning electron microscope and JEOL/JEM 2100 transmission electron microscope respectively.

The photocatalytic measurements were carried out using LZC-4X-Luzchem photoreactor with UV light intensity 600 lux and for the solar photocatalysis, the natural sunlight was found to be of 50,000-70000 lux intensity. The standard measurement of sunlight intensity¹⁴ was performed using Lutron, LX-107HA lux meter at Calicut University Campus, Kerala, India (Altitude: 11° 7' 34" North 75° 53' 25" East, Time: 11.00-12.30, Temperature: 26 ± 1 °C) on 1st July 2015. The dissolved oxygen concentration (DOC) in dye solution were calculated using EUTECH, Cyberscan DO 110 Dissolved Oxygen Meter.

Results and Discussion

In order to architect the light harvesters, oxygen rich yellow anatase TiO₂ (YAT-150) and oxygen vacancy rich black anatase TiO₂ (BAT-150), a sol-gel assisted microwave technique was designed, which is schematically represented in Figure 1. As the Figure 1 depicts, the *in situ* Mn (II) modification led the path to black anatase TiO₂ at a temperature 150 °C whereas the oxygen rich anatase TiO₂ (YAT-150) was obtained without using Mn (II). Both the samples have shown a glittering behaviour (Digital photographs of anatase TiO₂ samples, S2).

X ray Diffraction. The X-ray diffraction patterns (Figure 2) of YAT-150 and BAT-150 confirms the formation of anatase TiO₂ (JCPDS 75-1537) and from Figure 2B the overall anatase peak texturing along all directions with respect to YAT-150 (Figure 2A) is observed. Interestingly two new anatase peaks along (103) and (213) directions are originated in BAT-150, those are unseen in YAT-150. These new high intense peaks along (103) and (213) planes proved the higher phase purity of black anatase TiO₂. Thus Mn²⁺ incorporation (also evident from absorbance spectra and XPS) into the anatase crystal lattice has directed towards the origin of these new anatase peaks along with peak texturing. Since the ionic radius of Mn²⁺ (0.83 Å)¹⁵ is greater than that of anatase Ti⁴⁺ (0.74 Å),¹⁶ Mn²⁺ forced to withdraw lattice oxygen leading to oxygen vacancies. This would have definitely contributed towards the *in situ* location of Mn²⁺ into the lattice site of anatase TiO₂ paved the way to oxygen vacancy richness. Although Mn²⁺ is larger in size than Ti⁴⁺, the incorporation was confirmed by the positive shift occurred in the XRD pattern after Mn²⁺ modification (inset of figure 2). Furthermore the (211) peak of YAT-150 disappeared and a high index anatase (105) peak was generated on account of the synergistic effects of thermodynamic and kinetic factors which controls the crystal nucleation.¹⁷ The Mn²⁺ modification tend to lower the Gibbs free energy on (105) orientation specifically, and thus stabilizes the distinct atomic configuration along (105) plane.¹⁷

FTIR Spectroscopy. FTIR spectra (Figure 3) shows a broad band around 550 cm⁻¹ for both oxygen rich and oxygen deficient anatase TiO₂. The assigned peaks for Ti-O-Ti and Mn-O stretching vibrations are usually present at 500 and 794 cm⁻¹^{18,19} respectively which are masked within the broad band present in the range 400-900 cm⁻¹. The Ti-OH vibrations are

generally present at 740 and 670 cm^{-1} may also be merged within the same broad band.²⁰ The bands at 3410 and 1631 cm^{-1} are due to -OH stretching and bending vibration.²¹ The peak at 1440 cm^{-1} could be ascribed to the stretching vibration of surface adsorbed CO_2 .²² A noticeable peak is also present at 1020 cm^{-1} is the characteristic peak of δ -(Ti-OH) deformation and this peak is more intense for BAT-150, showing the highly deformed crystal lattice of BAT-150.²³

UV-Visible Absorption Spectroscopy and Tauc Plot. For YAT-150, the wavelength cut-off was found to be 520 nm (Figure 4B) whereas the absorption of BAT-150 (Figure 4C) is beyond the near IR (NIR) region. The former is due to oxygen richness and the latter is obviously because of the origin of oxygen vacancy richness with Ti^{3+} doping arose due to Mn^{2+} modification. These absorption features have definitely provided a positive contribution towards the higher photocatalytic efficiency of TiO_2 nanoparticles that have been synthesized. As compared to these, the standard Degussa-P25 photocatalyst has wavelength cut-off in the UV region (Figure 4A). The presence of absorption humps for BAT-150 in the range of 362–385 nm and 530–680 nm were associated with d-d electronic transitions of Mn^{2+} in the octahedral environment.²⁴ The absorption in the narrower range 360–385 nm is assigned to $6A_{1g}(S) \rightarrow 4E_g(D)$ and $4A_{1g} \rightarrow 4T_{2g}(D)$ transitions $4A_{1g} \rightarrow 4T_{1g}(G)$ transition reveals the incorporation of Mn^{2+} alone into the TiO_2 lattice.²⁴ In Tauc plot (Figure 5) the band gap energy for YAT-150 is 3.02 eV which abruptly decreased to 1.72 eV for BAT-150, which is attributed to the high reduction capability of Mn^{2+} which has introduced defects into the crystal lattice of TiO_2 directed towards the ultra-narrowed band gap. The reducing agent Mn^{2+} enters into the oxygen rich anatase titania, YAT-150 and accept the excess oxygen cloud leading to BAT-150, the Ti^{3+} doped black anatase titania.

XPS Analysis. XPS analysis of YAT-150 (Figure 6A) shows that $\text{Ti}2p_{3/2}$ and $\text{Ti}2p_{1/2}$ peaks are at 460.05 and 465.65 eV. These values are reduced to 457.65 and 462.65 eV respectively for BAT-150. For YAT-150, $\text{Ti}2p_{3/2}$ peak at 460.05 eV is obviously due to oxygen richness present in the sample¹² whereas for BAT-150 the same peak is negatively shifted to 457.65 eV attributes the oxygen vacancy richness (Ti^{3+} doping). In the $\text{Mn}2p$ spectrum (Figure 6B), where the binding energy peaks are observed at 640.55, 644.14, 651.95 eV and a satellite peak at 646.95 eV shows the evidence for Mn^{2+} doping alone into the crystal lattice of BAT-150.²⁵ Presence of these peaks establishes the responsibility for the negative peak shifting occurred for $\text{Ti}2p_{3/2}$ towards 457.65 eV in BAT-150 and also confirms the Ti^{3+} doped oxygen vacancy rich environment.²⁶ Simultaneously the oxidation state of Ti approaches to +3 from +4 ($\text{Ti}^{4+} \rightarrow \text{Ti}^{3+}$). In the $\text{O}1s$ XPS, the highest binding energy peak corresponding to Ti-O-Ti at 531.35 eV of YAT-150, is negatively shifted to 528.65 eV for BAT-150, which is attributed to the change in oxygen environment^{13, 27} as shown in Figure 6C. The peak at 533.85 and 535.85 eV for YAT-150 proved the

presence of Ti-OH and OH due to surface adsorbed water molecule respectively. For BAT-150, these peaks are shifted to 531.15 and 532.85 eV.^{28, 29} The splitting between $\text{Ti}2p_{3/2}$ and $\text{Ti}2p_{1/2}$ is found to be 5.6 eV for YAT-150 which could be assigned that TiO_2 is in the anatase phase.³⁰ After Mn^{2+} modification the peak separation was decreased to 5 eV which could be assigned to the peak texturing, peak formation and the band gap reduction occurred within Ti^{3+} doped black anatase TiO_2 (BAT-150).

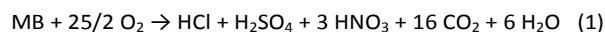
The band gap narrowing occurred due to the transformation from YAT-150 to BAT-150 (from 3.02 to 1.72 eV) as discussed earlier under absorption spectroscopy is due to the mid gap band generation and which is revealed from XPS analysis. Mid gap band states are either above the valence band (VB) or below the conduction band (CB). These mid band states will overlap with the respective band (VB or CB) leading to the reduction in band gap energy.¹¹ Here the valence band edge is observed at 2.01 eV and 4.15 eV for YAT-150 and BAT-150, below the Fermi energy confirms the substantial upward binding shift of 2.14 eV by introducing oxygen vacancy richness and simultaneous Ti^{3+} doping into the oxygen rich environment (Figure 7). Since the optical band gap of YAT-150 is 3.02 eV, the conduction band minimum would occur at -1.01 eV as depicted in the DOS diagram (Figure 8). From Figure 8, the oxygen vacancy rich TiO_2 (BAT-150) displays a conduction band minimum at 2.43 eV. The increase in VB maximum is due to the increased oxygen vacancy richness. The degree of oxygen richness is diminished here, which is evident from the XPS spectra i.e. the VB maximum colossally increased from 2.01 eV to 4.15 eV (from YAT-150 to BAT-150). These features can be easily perceived from DOS diagram.

TEM Analysis. The particle size of YAT-150 and BAT-150 are in the nanometer range and is confirmed from TEM studies (Figure 9A and 9B). The TEM studies revealed that both YAT-150 and BAT-150 are ultra-small nanoparticles having size around 5 nm. No considerable change in size and shape is observed due to variation in oxygen concentration. The HRTEM images are also displayed here (Figure 9C and Figure 9D) and the fringe spacing (d) of YAT-150 and BAT-150 were found to be 0.340 and 0.339 nm respectively, which are exactly in correct agreement with that of (101) plane of anatase TiO_2 standard data (JCPDS 75-1537).³¹ The corresponding SAED patterns were also displayed inset to show the sharp diffraction pattern and high anatase phase purity.

Photocatalysis. In order to examine the photocatalytic activity of YAT-150 and BAT-150, methylene blue dye degradation measurements were carried out both under natural sunlight and UV light are shown in Figure 10. The absorption spectra of methylene blue shows two peaks at 614 and 662 nm (The UV-Visible absorption spectra for degradation for all samples including Degussa-P25 are shown in Figure S6 & S7) which could be assigned to methylene blue dimer and monomer peak respectively.³² The photocatalysis under natural sunlight was performed using YAT-150, BAT-150 and Degussa-P25. The

results have projected a captivating outlook for YAT-150 and BAT-150 that have been synthesized by sol-gel assisted microwave strategy. The photodegradation of the dye occurred within 40 and 20 minutes for YAT-150 and BAT-150 respectively, whereas the commercially available Degussa-P25 photocatalyst has completed the catalytic process by taking more than 90 minutes.

Generally the photooxidation of methylene blue dye occurs under aerobic conditions, where the amount of dissolved oxygen is sufficient to enhance the photocatalytic process along with the photocatalysts by trapping the electrons that are formed by the photoexcitation of the valence band of TiO₂. The photooxidation reaction under aerobic conditions can be described by the following equation.^{33,34}



Besides the oxidation process, demethylation process can also be occur during dye degradation.³⁵ In the present work, all the photocatalytic measurements were carried out in presence of air to supply sufficient molecular oxygen. The dissolved oxygen concentration (DOC) measurements have been done and the average DOC values during the photocatalytic processes were shown in Table 1. This higher concentration of dissolved oxygen in the photocatalytic reaction mixture would have undoubtedly paved the way to enhance the photocatalytic efficiency by trapping the conduction band electron leading to the formation of super oxide radicals (O₂^{-•}) by reduction. The so formed super oxide (O₂^{-•}) and hydroxyl (OH•) radicals that has been formed due to the reaction between water and the hole generated at the TiO₂ valence band jointly facilitate the photo destruction of the methylene blue dye.³⁶

These photocatalytic aspects confirmed the remarkable activity of both YAT-150 and BAT-150. BAT-150 is twice active than that of YAT-150. In addition to this, the photocatalytic activity of YAT-150 and BAT-150 were found to be 2-fold and 4-fold active to that of Degussa-P25 photocatalyst. In presence of UV illumination, YAT-150 has performed photodegradation within 210 minutes whereas BAT-150 have taken only 180 minutes. However, Degussa-P25 have shown the highest photocatalytic activity under UV light owing to its wide area absorption under UV region and the mixed phase behaviour. The higher adsorption capability of Degussa-P25 as compared to YAT-150 and BAT-150 (Figure S1) facilitated higher photocatalytic efficiency of Degussa-P25 under UV irradiation. Degussa-P25 contains 75% anatase and 25% rutile phases and its high photocatalytic activity has been reported elsewhere.^{37,38} BAT-150 has utilized the first 60 minutes for monomer-dimer equilibration (decrease in monomer peak alone) and thereafter the degradation was jointly concerted (The UV-Visible absorption spectra of dye degradation, Figure. S6.B). The dimerization may facilitate the hazardous activity inhibition of toxic active sites. Obviously, the active sites of organic pollutants are initially restrained by keeping dimerized moieties prior to degradation. For certain, the degradation was performed within 120 minutes. A hypsochromic shift is

observed in all the catalytic processes, which is attributed to N-demethylation (Figure S6 & S7).³²

Conclusion

A green and rapid sol-gel assisted microwave strategy is established for the synthesis of oxygen rich yellow anatase TiO₂ and Ti³⁺ doped oxygen vacancy rich black anatase TiO₂. As synthesized black and yellow anatase TiO₂ nanoparticles were characterized by XRD, TEM, XPS, FTIR and UV-VIS spectroscopy. XRD studies revealed the origin of new anatase peaks along (103), (213) and (105) direction with peak texturing in black anatase TiO₂ as compared to the yellow coloured anatase TiO₂. The anatase phase pure yellow and black TiO₂ nanoparticles were of ultra-small size (~5 nm) confirmed by TEM analysis. XPS studies evidently demonstrated the occurrence of a large upward binding shift of 2.14 eV as the anatase TiO₂ changed its environment from oxygen richness to oxygen vacancy richness. These yellow and black anatase TiO₂ nanoparticles were employed as solar photocatalysts and compared their activity with commercially available Degussa-P25. The photocatalytic efficiencies of yellow and black anatase TiO₂ were two-fold and four-fold active than the commercially available photocatalyst, Degussa-P25.

Acknowledgements

The authors Sanjay G. Ullattil is grateful to UGC-BSR fellowship, F.7-184/2007(BSR), FD Diary No. 717 and Pradeepan Periyat is thankful to UGC, India [(Grant no F.20-6(8)-2012(BSR))] for providing financial support.

Notes and references

- J. Tian, Z. Zhao, A. Kumar, R. I. Boughton and H. Liu, *Chem. Soc. Rev.*, 2014, **43**, 6920-6937.
- L. Sun, Z. Zhao, Y. Zhou and L. Liu, *Nanoscale*, 2012, **4**, 613-620.
- J. Yu, J. Fan and K. Lv, *Nanoscale*, 2010, **2**, 2144-2149.
- P. Periyat, N. Leyland, D. E. McCormack, J. Colreavy, D. Corr and S. C. Pillai, *J. Mater. Chem.*, 2010, **20**, 3650-3655.
- S. Afzal, W. A. Daoud and S. J. Langford, *J. Mater. Chem. A*, 2014, **2**, 18005-18011.
- X. Chen and C. Burda, *J. Am. Chem. Soc.*, 2008, **130**, 5018-5019.
- S. Bingham and W. A. Daoud, *J. Mater. Chem.*, 2011, **21**, 2041-2050.
- P. Periyat, K. V. Baiju, P. Mukundan, P. K. Pillai and K. G. K. Warriar, *J. Sol-Gel Sci. Technol.*, 2007, **43**, 299-304.
- J. C. Yu, W. Ho, J. Yu, H. Yip, P. K. Wong and J. Zhao, *Environ. Sci. Technol.*, 2005, **39**, 1175-1179.
- X. Chen, L. Liu and F. Huang, *Chem. Soc. Rev.*, 2015, **44**, 1861-1885.
- X. Chen, L. Liu, Y. Y. Peter and S. S. Mao, *Science*, 2011, **331**, 746-750.
- L. L. Tan, W. J. Ong, S. P. Chai and A. R. Mohamed, *Chem. Commun.*, 2014, **50**, 6923-6926.
- V. Etacheri, M. K. Seery, S. J. Hinder and S. C. Pillai, *Adv. Funct. Mater.*, 2011, **21**, 3744-3752.

- 14 S. Thakur and N. Karak, *J. Mater. Chem. A*, 2015, **3**, 12334-12342.
- 15 B. Murugan and A. V. Ramaswamy, *J. Phys. Chem. C*, 2008, **112**, 20429-20442.
- 16 Z. V. Saponjic, N. M. Dimitrijevic, O. G. Poluektov, L. X. Chen, E. Wasinger, U. Welp, and T. Rajh, *J. Phys. Chem. B*, 2006, **110**, 25441-25450.
- 17 H. B. Jiang, Q. Cuan, C. Z. Wen, J. Xing, D. Wu, X. Q. Gong and H. G. Yang, *Angew. Chem. Inter. Ed.*, 2011, **50**, 3764-3768.
- 18 S. C. Pillai, P. Periyat, R. George, D. E. McCormack, M. K. Seery, H. Hayden and S. J. Hinder, *J. Phys. Chem. C*, 2007, **111**, 1605-1611.
- 19 D. Wang, J. Huang, X. Li, P. Yang, Y. Du, C. M. Goh and C. Lu, *J. Mater. Chem. A*, 2015, **3**, 4195-4202.
- 20 L. Shao, L. Zhang, M. Chen, H. Lu and M. Zhou, *Chem. Phys. Lett.*, 2011, **343**, 178-184.
- 21 R. Nakamura, A. Imanishi, K. Murakoshi and Y. Nakato, *J. Am. Chem. Soc.*, 2003, **125**, 7443-7450.
- 22 N. T. Nolan, M. K. Seery and S. C. Pillai, *J. Phys. Chem. C*, 2009, **113**, 16151-16157.
- 23 T. Bezrodna, G. Puchkovska, V. Shymanovska, J. Baran and H. Ratajczak, *J. Mol. Struct.*, 2004, **700**, 175-181.
- 24 B. S. Reddy, N. O. Gopal, K. V. Narasimhulu, C. L. Raju, J. L. Rao and B. C. V. Reddy, *J. Mol. Struct.*, 2005, **751**, 161-167.
- 25 M. C. Biesinger, B. P. Payne, A. P. Grosvenor, L. W. Lau, A. R. Gerson and R. S. C. Smart, *Appl. Surf. Sci.*, 2011, **257**, 2717-2730.
- 26 S. Rtimi, J. Nestic, C. Pulgarin, R. Sanjines, M. Bensimon and J. Kiwi, *Interface focus*, 2015, **5**, 20140046.
- 27 R. Ren, Z. Wen, S. Cui, Y. Hou, X. Guo and J. Chen, *Sci. Rep.*, 2015, **5**, 10714.
- 28 T. Leshuk, R. Parviz, P. Everett, H. Krishnakumar, R. A. Varin and F. Gu, *Appl. Mater. Interface.*, 2013, **5**, 1892-1895.
- 29 M. M. Khan, S. A. Ansari, D. Pradhan, M. O. Ansari, J. Lee and M. H. Cho, *J. Mater. Chem. A*, 2014, **2**, 637-644.
- 30 T. Harifi and M. Montazer, *Appl. Catal. A: Gen.*, 2014, **473**, 104-115.
- 31 P. Periyat, P. A. Saeed and S. G. Ullattil, *Mater. Sci. Semicond. Process.*, 2015, **31**, 658-665.
- 32 D. P. DePuccio, P. Botella, B. O'Rourke and C. C. Landry, *ACS Appl. Mater. Interface.*, 2015, **7**, 1987-1996.
- 33 A. Houas, H. Lachheb, M. Ksibi, E. Elaloui, C. Guillard and J. M. Herrmann, *Appl. Catal. B: Environ.*, 2001, **31**, 145-157.
- 34 C. Yogi, K. Kojima, N. Wada, H. Tokumoto, T. Takai, T. Mizoguchi and H. Tamiaki, *Thin Solid Films*, 2008, **516**, 5881-5884.
- 35 T. Zhang, T. Oyama, A. Aoshima, H. Hidaka, J. Zhao and N. Serpone, *J. Photochem. Photobiol. A: Chem.*, 2001, **140**, 163-172.
- 36 J. Yu, X. Zhao and Q. Zhao, *Thin Solid Films*, 2000, **379**, 7-14.
- 37 D. C. Hurum, A. G. Agrios, K. A. Gray, T. Rajh and M. C. Thurnauer, *J. Phys. Chem. B*, 2003, **107**, 4545-4549.
- 38 V. Puddu, H. Choi, D. D. Dionysiou and G. L. Puma, *Appl. Catal. B: Environ.*, 2010, **94**, 211-218.

Figures – manuscript id: NR-ART-09-2015-005975

Green Microwave Switching from Oxygen Rich Yellow Anatase to Oxygen Vacancy Rich Black Anatase TiO₂ Solar Photocatalyst Using Mn (II) as ‘Anatase Phase Purifier’

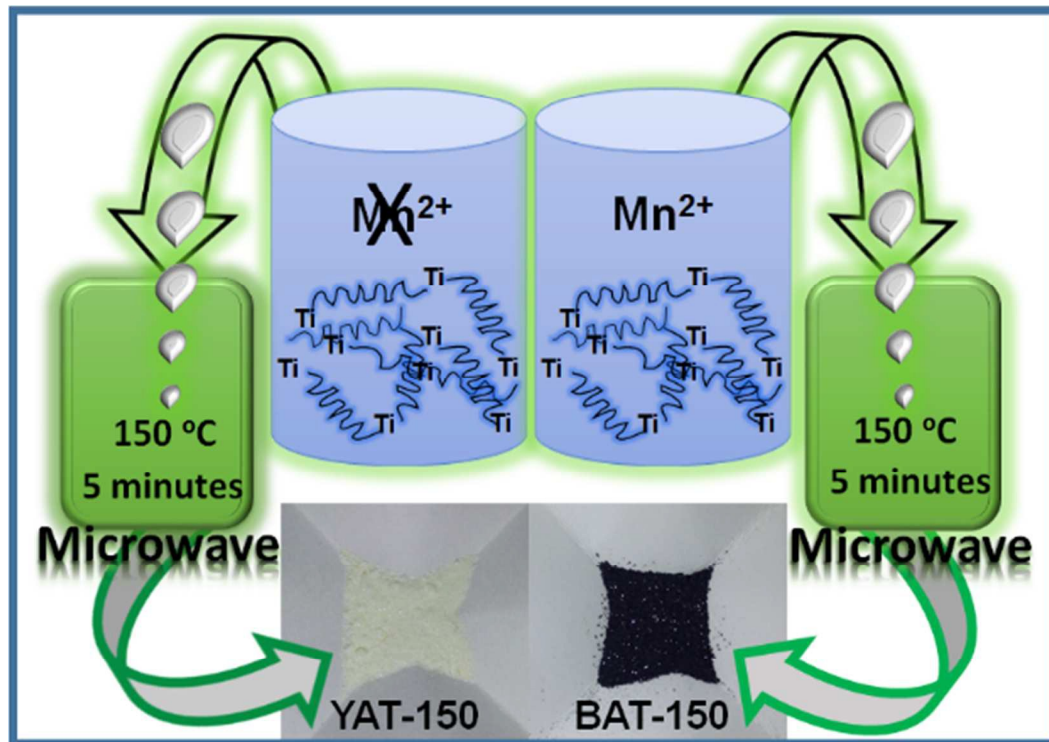


Figure 1. Schematic illustration of the synthesis of yellow and black anatase TiO₂

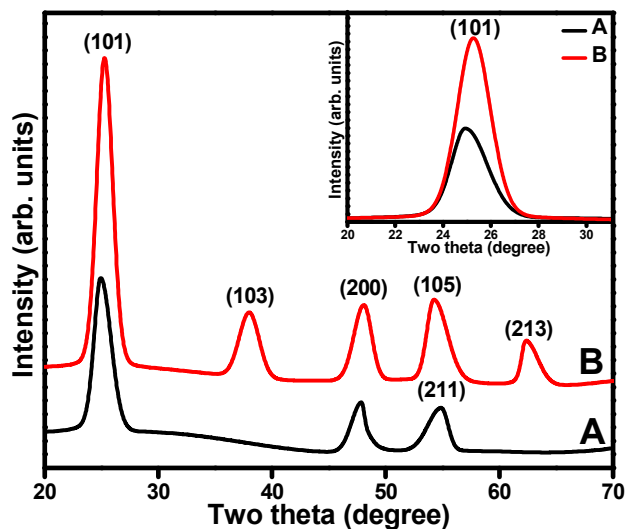


Figure 2. X ray diffraction pattern of A) YAT-150 and B) BAT-150. (Inset shows the peak shift and peak intensity variation (A) before and (B) after Mn^{2+} reduction)

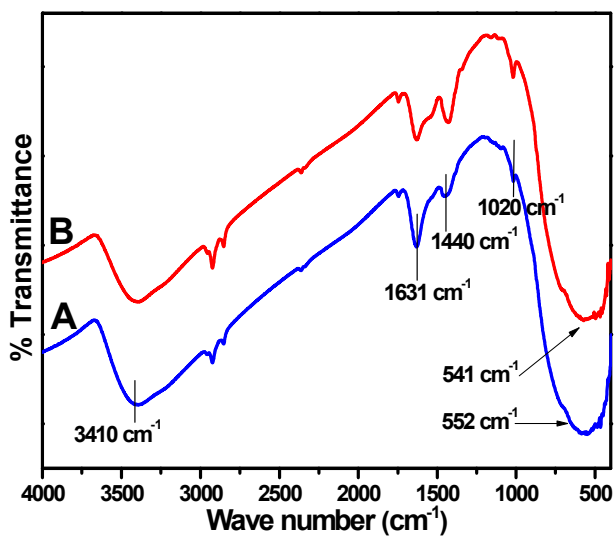


Figure 3. FTIR spectra of A) YAT-150 and B) BAT-150.

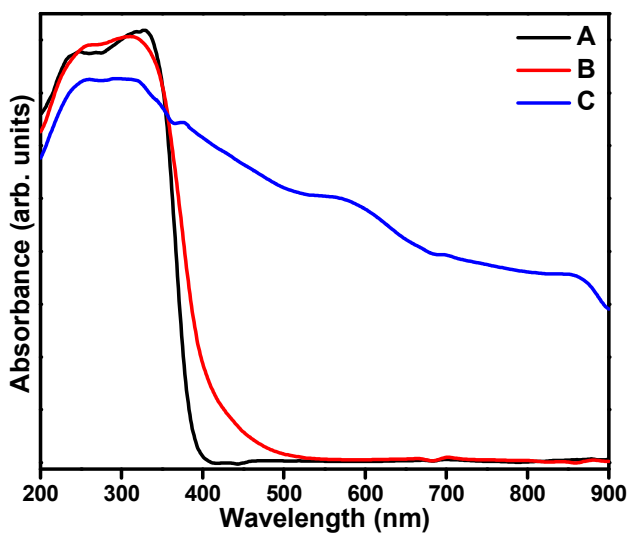


Figure 4. UV-Visible absorption spectra of A) Degussa-P25 B) YAT-150 and C) BAT-150.

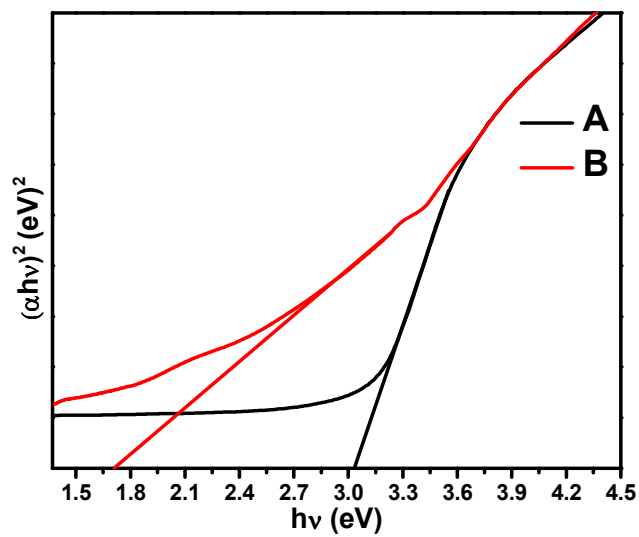


Figure 5. Tauc plot of A) YAT-150 and B) BAT-150

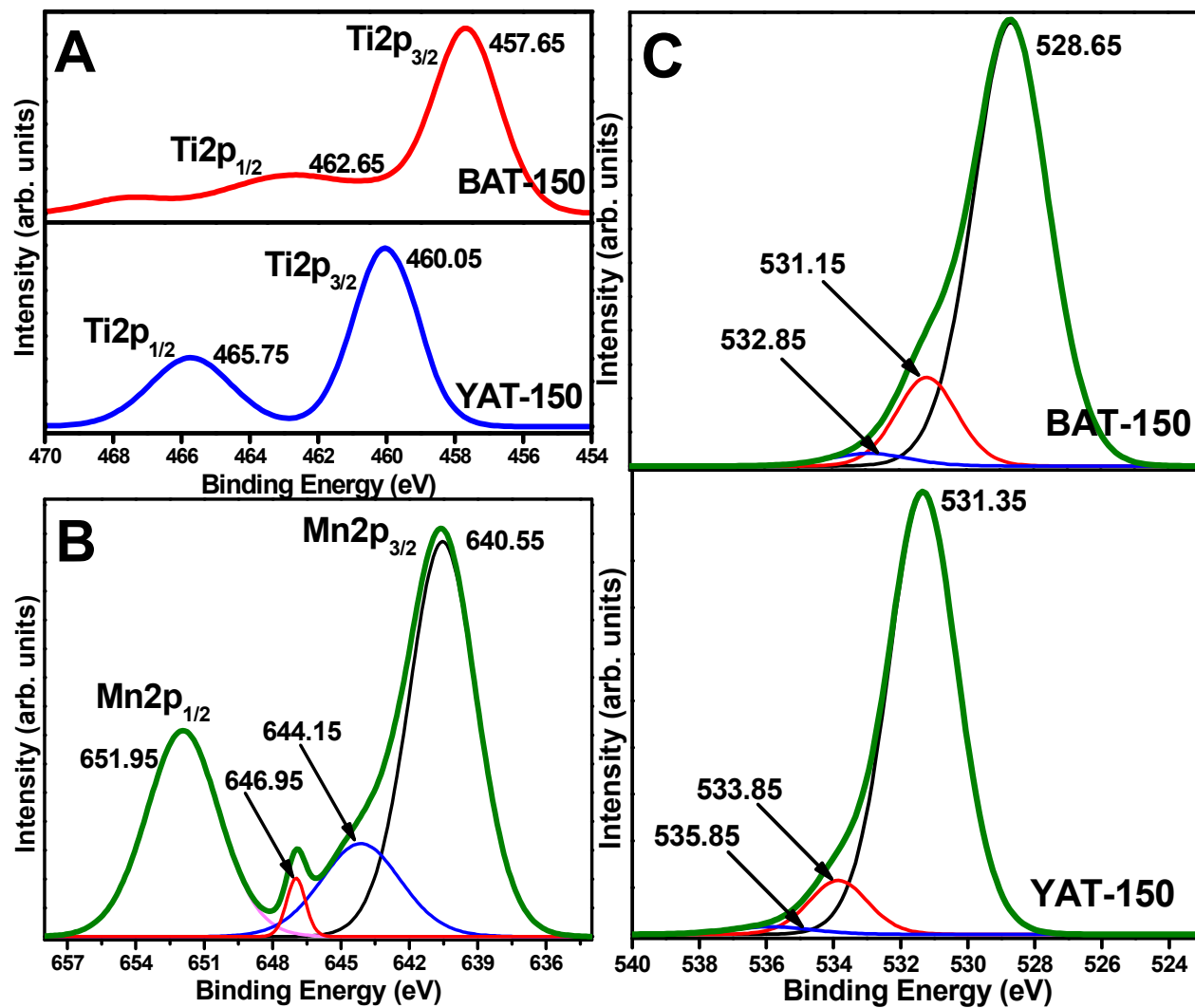


Figure 6. XPS spectra of A) Ti2p of YAT-150 and BAT-150 B) Mn2p of BAT-150 C) O1s of YAT-150 and BAT-150.

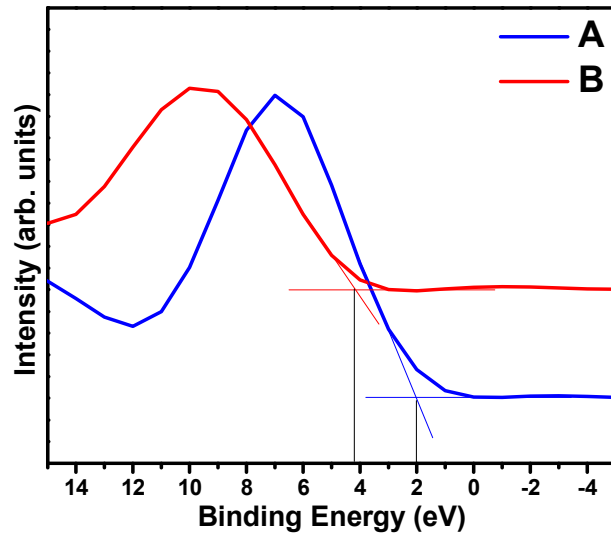


Figure 7. The Valence band spectra of A) YAT-150 and B) BAT-150.

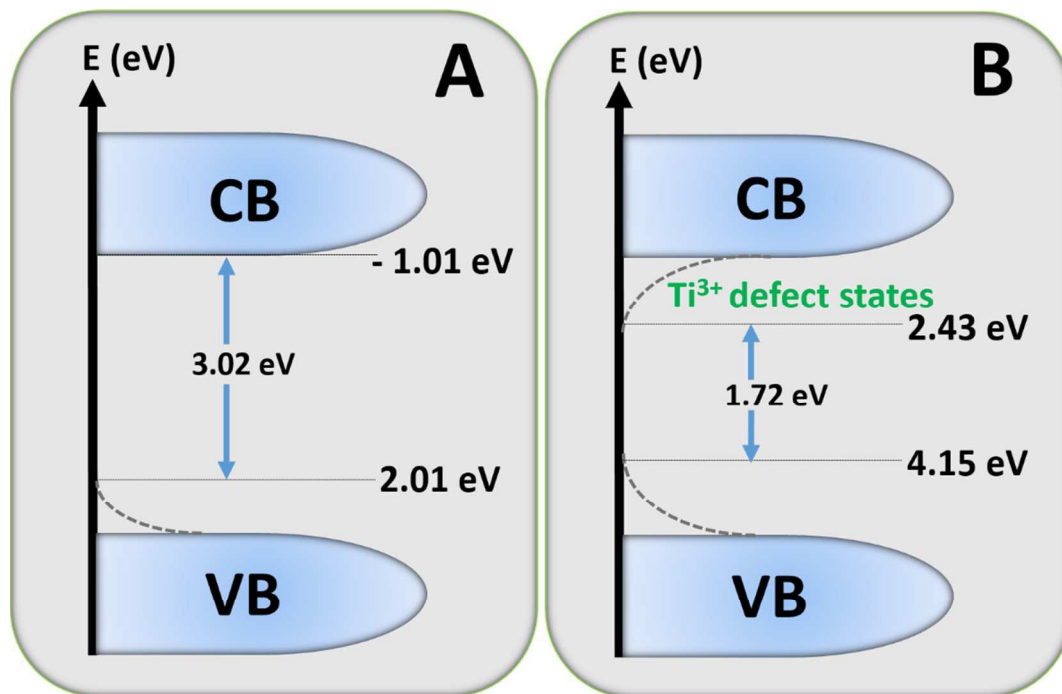


Figure 8. Density of States (DOS) for A) YAT-150 and B) BAT-150.

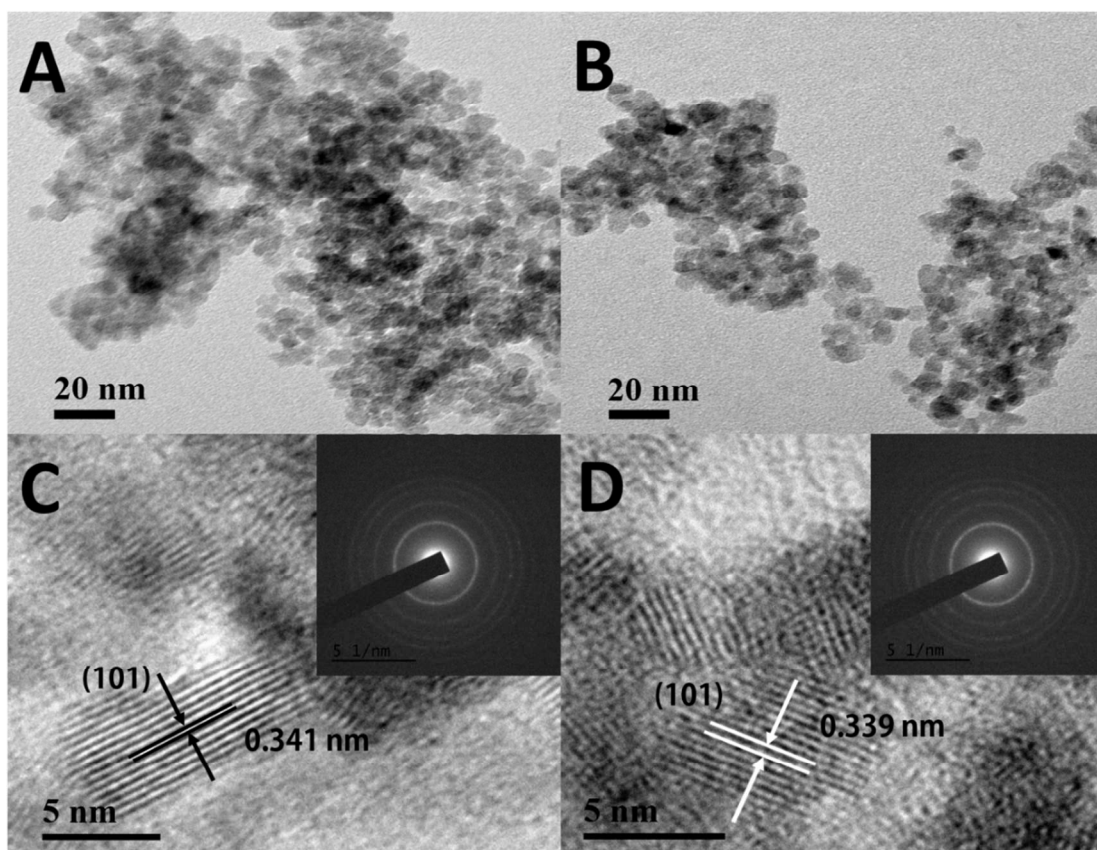


Figure 9. TEM images of A) YAT-150, B) BAT-150 and HRTEM images of C) YAT-150 D) BAT-150.

Table 1. Dissolved Oxygen Concentration in the MB dye solution during photocatalysis (mg/L)

YAT – 150		BAT – 150		Degussa – P25	
UV	SUNLIGHT	UV	SUNLIGHT	UV	SUNLIGHT
5.42	5.37	5.65	5.43	5.96	4.95

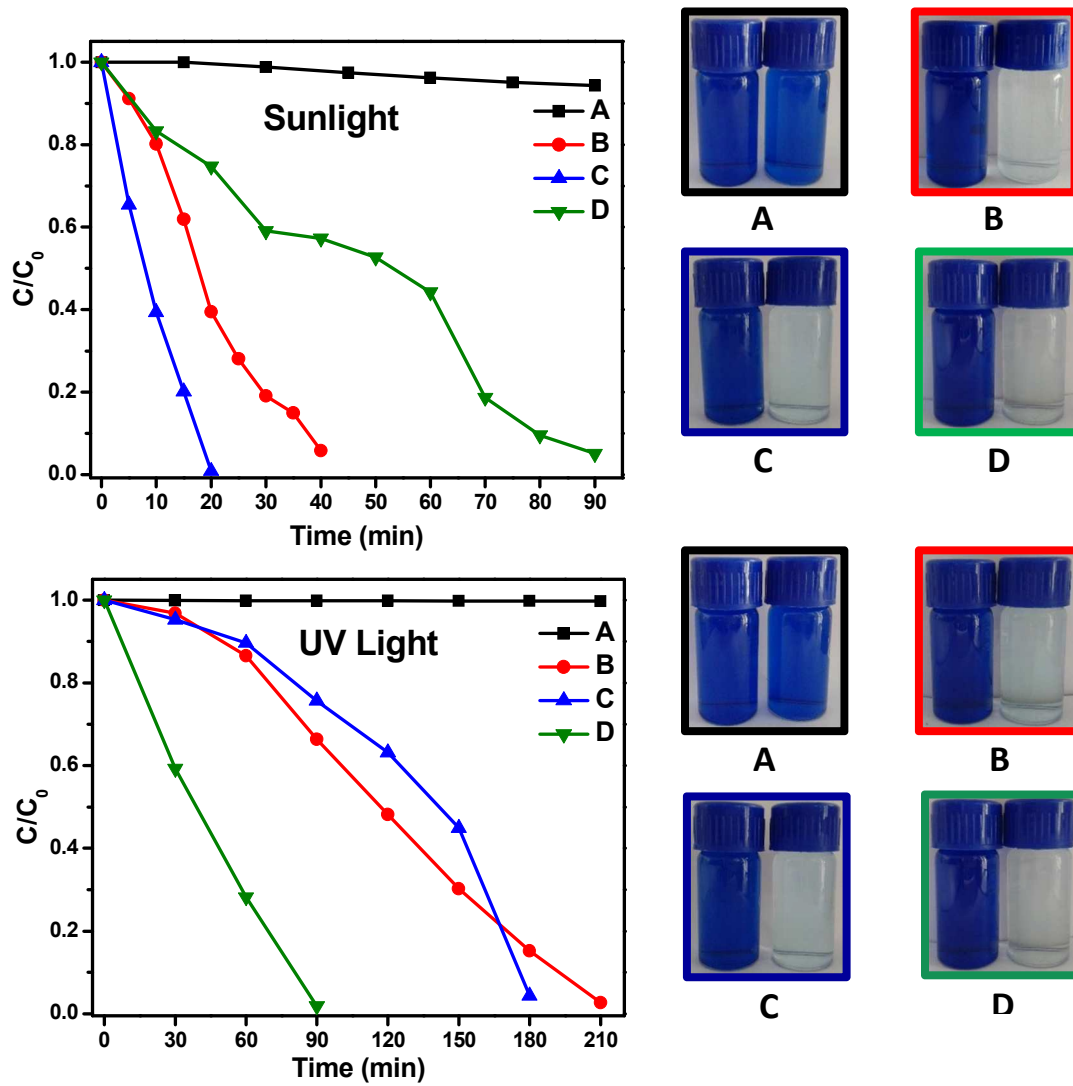


Figure 10. Photodegradation plot of methylene blue dye degradation under sunlight and UV light using A) No catalyst B) Degussa- P25, C) YAT-150 and D) BAT-150.